Electronic Supplementary Material (ESI) for Journal of Materials Chemistry A.
This journal is © The Royal Society of Chemistry 2019

ELECTRONIC SUPPLEMENTARY INFORMATION (ESI†)

Streptavidin Activated Hydroxyl radicals Enhanced Photocatalytic and Photoelectrochemical Properties of Membrane-bound like $CaMoO_4:Eu^{3+}$ Hybrid Structures

Eluri Pavitra[a], *Ganji Seeta Rama Raju*[b], *Seyed Majid Ghoreishian*[a], *L. Krishna Bharat*[c,f], *Sreekantha Reddy Dugasani*[d], *Jin Young Park*[e], *Sung Ha Park*[d], *Jae Su Yu**[c], *Young-Kyu Han**[b], *Yun Suk Huh**[a]

[a]*Department of Biological Engineering, Biohybrid Systems Research Center (BSRC), Inha University, Incheon, 22212, Republic of Korea*

[b]*Department of Energy and Materials Engineering, Dongguk University-Seoul, Seoul 04620, Republic of Korea*

[c]*Department of Electronic Engineering, Institute for Wearable Convergence Electronics, Kyung Hee University, Yongin-si, Gyenggi-do-17104, Republic of Korea*

[d]*Department of Physics and Sungkyunkwan Advanced Institute of Nanotechnology (SAINT), Sungkyunkwan University, Suwon 16419, Republic of Korea*

[e]*Department of Electrical, Electronics and Software Engineering, Pukyong National University, Yongdang Campus, Busan, 48547, Republic of Korea*

[f]*Center of Biomedical Engineering, Institute of Molecular Medicine, Sechenov University, Moscow 119991, Russia*

Address Correspondence to

**E-mail: jsyu@khu.ac.kr (Prof. J. S. Yu) ykenergy@dongguk.edu (Prof. Y.-K. Han) yunsuk.huh@inha.ac.kr (Prof. Y. S. Huh)*

Characterizations

The morphologies of the $CaMoO_4:Eu^{3+}$ and SA-$CaMoO_4:Eu^{3+}$ samples were perceived using high-resolution field-emission scanning electron microscope (HR FE-SEM, Hitachi-SU8010, Japan) and field-emission transmission electron microscope (FE-TEM, JEOL, JEM-2100F, Japan). Elemental mapping was conducted using the energy dispersive X-ray spectroscopy (EDS), which was attached to the SEM instrument. The powder X-ray diffraction (XRD) patterns of all the samples were measured at room temperature on X'Pert Pro MRD (PANalytical, Holland) system. FTIR analysis was performed by recording the IR spectrum between 400-4000 cm^{-1} of SA-$CaMoO_4:Eu^{3+}$ microstructures on a JASCO FT/IR-6600 spectrometer. The electronic states of elements presented in the SA-$CaMoO_4:Eu^{3+}$ were obtained with the help of XPS (K-alpha XPS, Thermo Scientific, USA) system. The room-temperature PL spectra were recorded on a Photon Technology International (PTI, USA) fluorimeter with a Xe-arc lamp of 60 W power and the lifetime was measured with a phosphorimeter attachment to the main system with 25 watt power Xe-flash lamp. Photocatalytic decolorization process was conducted in a closed photoreactor comprising a cylindrical vessel made of pyrex glass which operated with an initial working volume of 200 ml. The radiation sources were three low-pressure mercury UV lamps (30 W, UV-A, manufactured by Philips, Holland), which were placed at top of the photoreactor and the distance between the mercury UV lamp and the solution was ≤ 10 cm. The internal body of the photoreactor was covered with an aluminum foil to reduce the radiation losses. The internal temperature was adjusted to 25 ± 1 °C. Total Organic Carbon (TOC) measurements were carried out in the TC/TIC measuring mode using a vario TOC cube (Elementar, Germany).

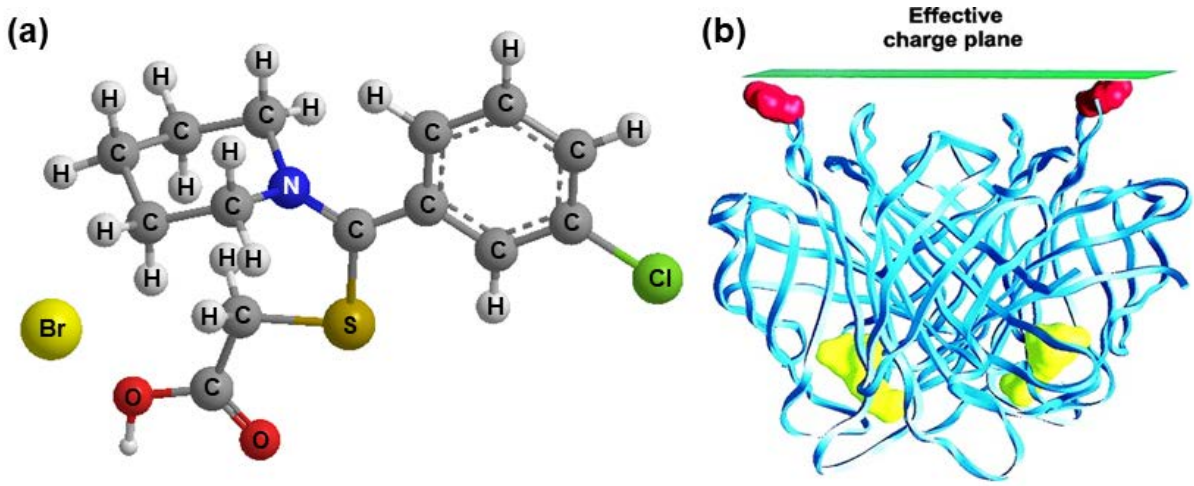

Fig. S1. (a) Chemical structure of SA and (b) location of effective charge plane (adopted from Ref. [22]).

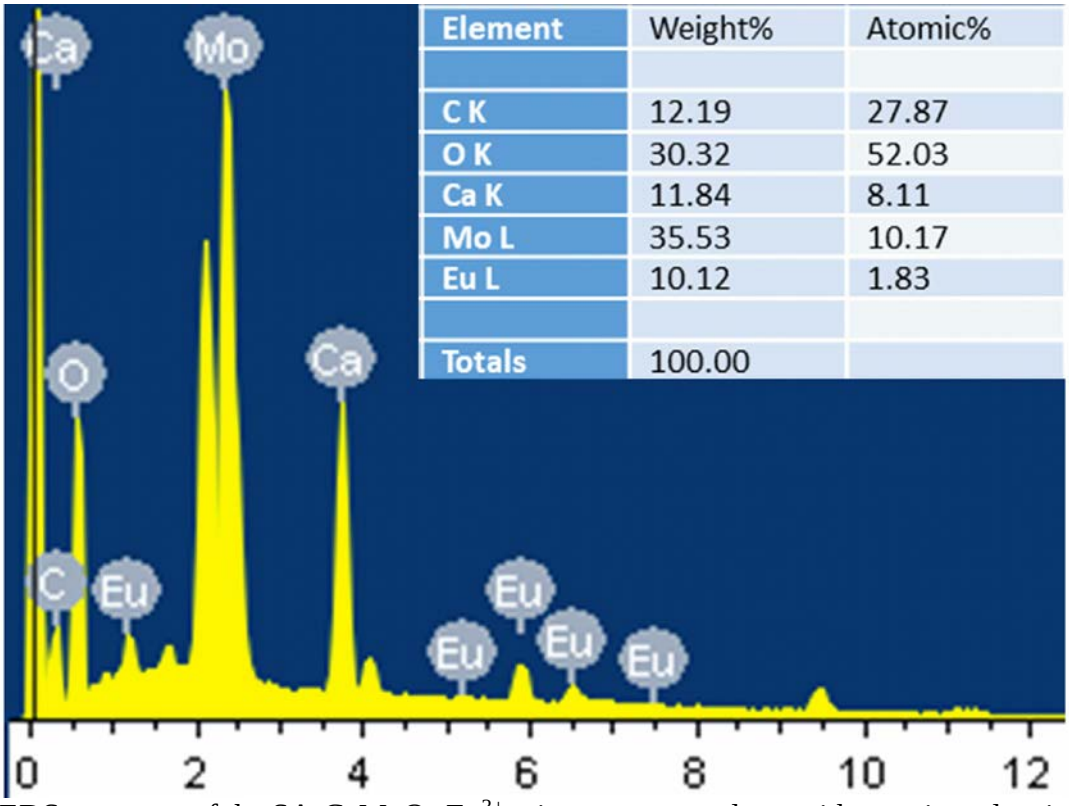

Element	Weight%	Atomic%
C K	12.19	27.87
O K	30.32	52.03
Ca K	11.84	8.11
Mo L	35.53	10.17
Eu L	10.12	1.83
Totals	100.00	

Fig. S2. EDS spectrum of the SA-$CaMoO_4$:Eu^{3+} microstructures along with atomic and weight percentages of the ions.

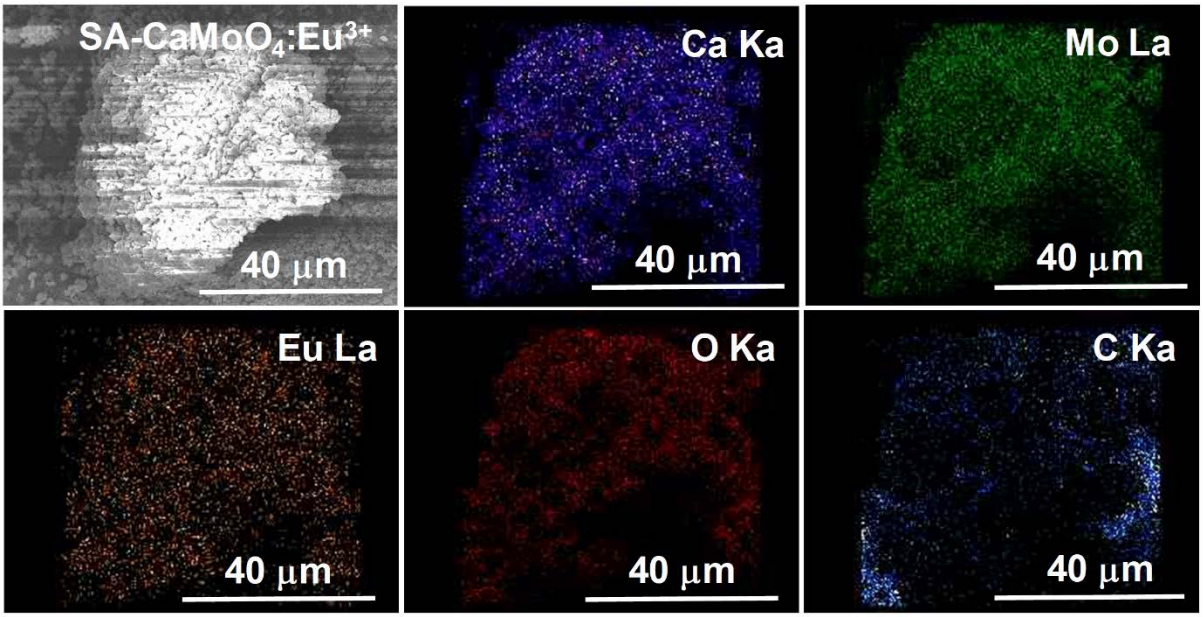

Fig. S3. Elemental mapping of the ions based on the EDS spectrum of the SA-$CaMoO_4$:Eu^{3+}**.**

Different concentrations (1, 3 and 5 ml) of DNA were co-modified with SA-$CaMoO_4:Eu^{3+}$ samples, and the change observed in the morphology is shown in Fig. S5. Initially, different DNA sequences (Salmon, R1(1-1), Cs(2-1) and Cs(2-2)) were individually doped in $CaMoO_4:Eu^{3+}$ host and the corresponding images are presented in Fig. S4a-d.

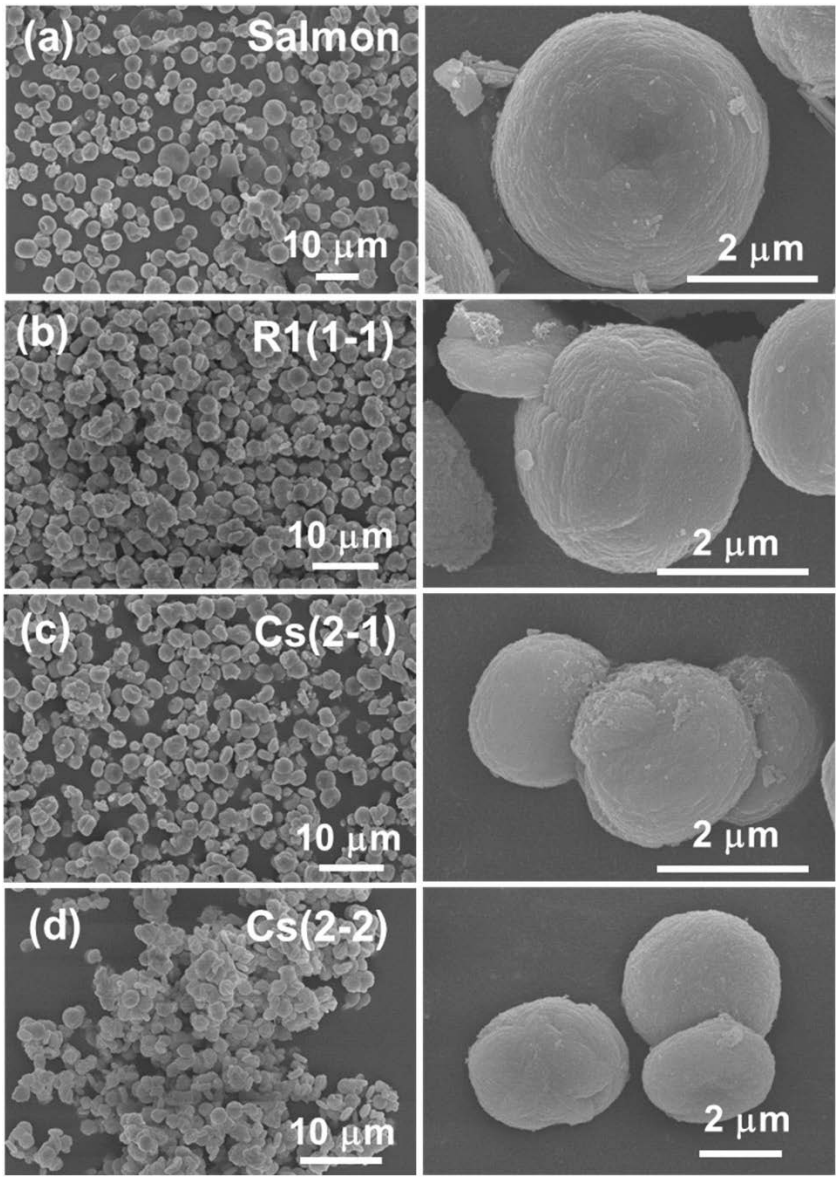

Fig. S4. FE-SEM images of different DNAs modified $CaMoO_4:Eu^{3+}$ samples (a) Salmon, (b) R1(1-1), (c) Cs(2-1), and (d) Cs(2-2) DNAs respectively.

The obtained morphology was almost similar to that of host morphology, which means

that DNA alone did not have any major impact on the morphology in our synthesis. However, salmon DNA-modified particles were well-dispersed and showed with less aggregation compared with the other samples. Besides, salmon DNA has demonstrated the potential to generate mechanically strong, biocompatible, and non-toxic devices in biological, physical, and medical applications.[1, 2] Therefore, we selected salmon DNA, and 50 µl streptavidin/1 ml DNA co-modified $CaMoO_4:Eu^{3+}$ microstructures (SA/DNA-$CaMoO_4:Eu^{3+}$) showed a sphere morphology, as presented in Fig. S5a.

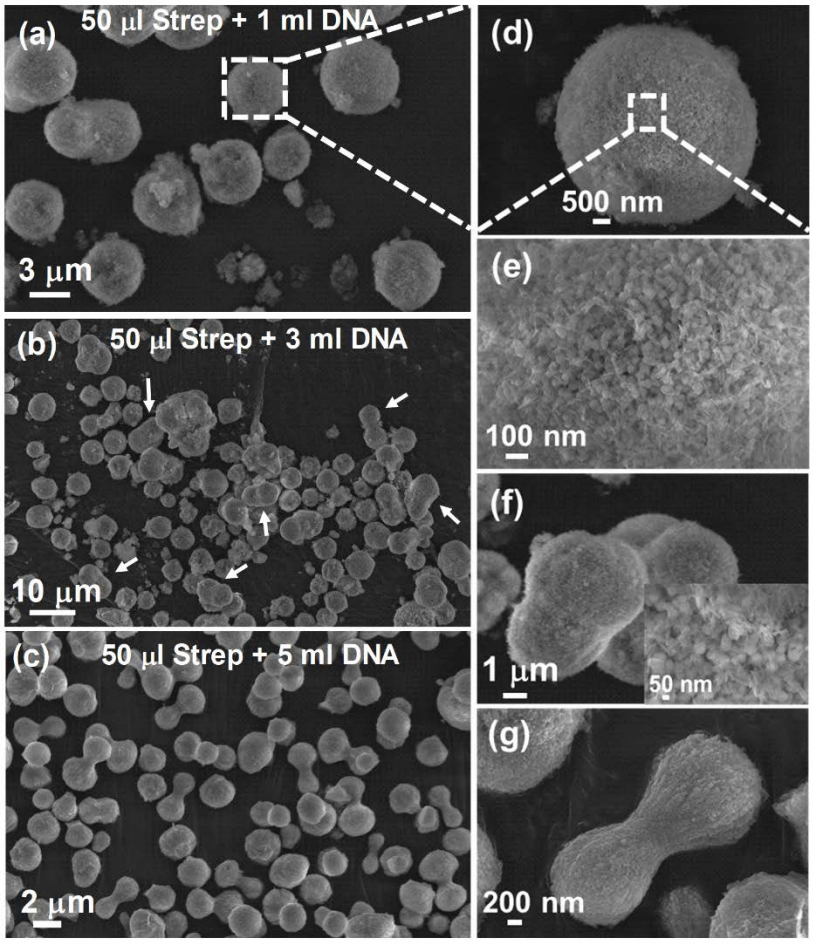

Fig. S5. FE-SEM images of SA-$CaMoO_4:Eu^{3+}$ microstructures co-modified with (a) 1 ml DNA, (b) 3 ml DNA, and (c) 5 ml DNA respectively. (d) & (e) are the corresponding magnified images of the Fig. (a). (f) & (g) are the corresponding high-resolution images of the (b) & (c) respectively.

Magnified images of a single particle and its surface morphology are shown in Fig. S5d and S5e, respectively. Based on the SEM images, spherical particles were constructed as a group of nanoparticles and their surface was covered with nanorods. In this co-modifying case, the DNA boosted the nucleation rate rather than crystal growth and helped to create numerous nucleating centers to form initial nuclei. Besides, DNA itself has self-assembling ability to construct periodic structures. Therefore, we can conclude that the nanoparticles self-assembled into spherical particles. Upon increasing the DNA concentration to 3 ml, the spherical particles combined with neighboring particles due to increased surface density as shown in Fig. S5b. The amount of nanorods covering the surface of the spherical particles increased, and nanorods aggregated with neighboring particles, as shown in Fig. S5f. Lastly, when 5 ml of DNA was co-modified along with SA, most of the particles acquired a dumbbell shape as shown in Fig. S5c and the magnified image of a single particle is presented in Fig. S5g. Therefore, in this case of SA/DNA-$CaMoO_4$:Eu^{3+} microstructures, DNA acted as a scaffolding material and organized self-assembly of the highly structured materials with specific nanoscale features.

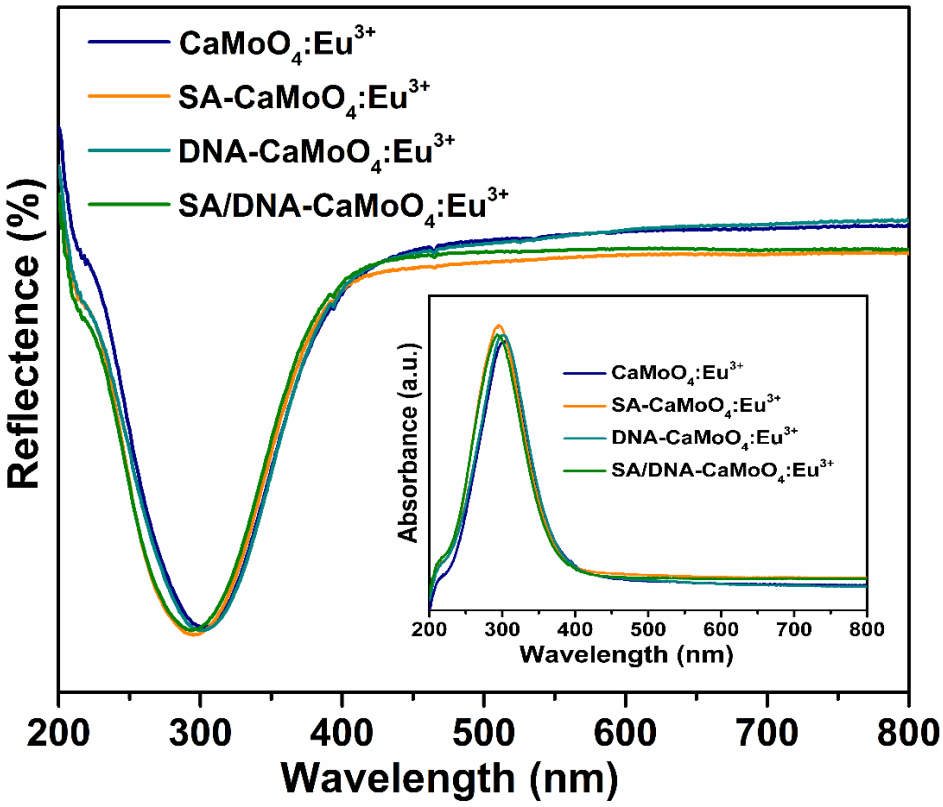

Fig. S6. UV-VIS diffuse reflectance spectra of $CaMoO_4:Eu^{3+}$ host, SA-$CaMoO_4:Eu^{3+}$, DNA-$CaMoO_4:Eu^{3+}$, and SA/DNA-$CaMoO_4:Eu^{3+}$ microstructures and the inset shows their corresponding absorption spectra.

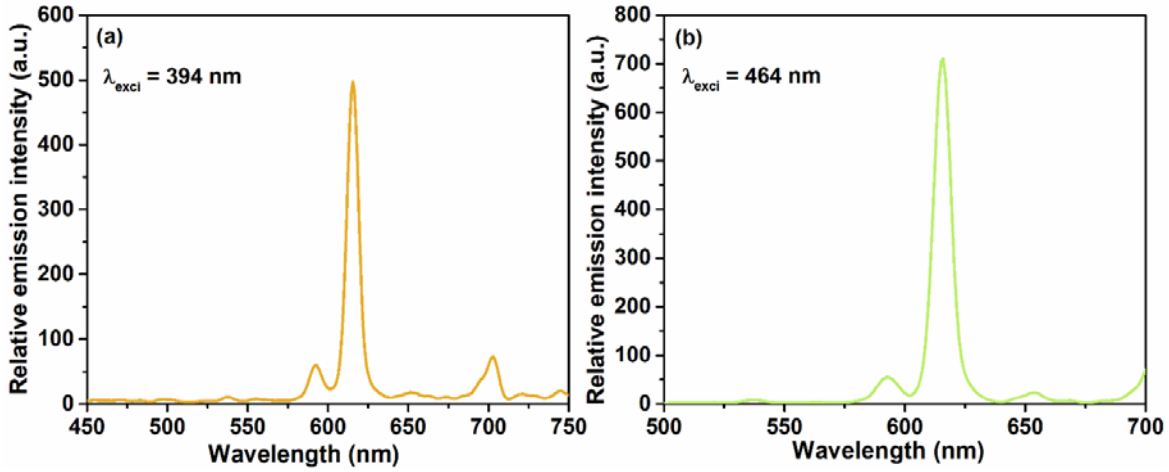

Fig. S7. PL emission spectra of $CaMoO_4:Eu^{3+}$ host at different excitation wavelengths of (a) 394 nm and (b) 464 nm.

Experimental design and mathematical modeling for photocatalysis:

In this study, CCD based RSM was applied to optimize the four operating variables (MB concentration (X_1), catalyst dosage (X_2), pH (X_3) and irradiation time (X_4)). *Y* is the predicted response for photocatalytic decolorization efficiency. The response model may be expressed according to the following equation:

$$Y = f(X_1, X_2, X_3, \ldots, X_n) \pm \varepsilon \quad (1)$$

Where *f* is the response function, X_i is the independent variable, and ε is the experimental error.

Coded and uncoded values of the four independent variables (X_1, X_2, X_3 and X_4) in CCD have been presented in the following Table S1.

Table S1. Experimental range and levels of the independent variables

Variables	Unit	Coded factor	Range and level				
			-α	-1	0	+1	+α
MB concentration	mg/L	X_1	5	11	18	24	30
Catalysts dosage	mg/100 ml	X_2	100	125	150	175	200
pH		X_3	2	4	6	8	10
Irradiation time	min	X_4	30	50	75	100	120

Factor levels were chosen to cover a range of values of practical interest. The four mentioned test factors were coded in the regression equation, according to the following equation:

$$x_i = \frac{X_i - X_{io}}{\Delta X_i} \quad (2)$$

where x_i is the coded value of the i^{th} independent variable, X_i is the natural value of the i^{th} independent variable, X_{io} is the natural value of the i^{th} independent variable at the center point, and ΔX_i is the step change value.[3] The optimal conditions for the decolorization process were determined by the response surface regression procedure to fit the following second-order polynomial model:

$$Y = \beta_0 + \sum_{i=1}^{k} \beta_i x_i + \sum_{i=1}^{k} \beta_{ii} x_i^2 + \sum_{i=1}^{k} \sum_{j=1}^{k} \beta_{ij} x_i x_j + \varepsilon \quad (3)$$

where x_i represents the effect of the independent variables. Similarly, x_i^2 is the square effects, β_0 is the constant, β_i is the slope or linear effect of the input factor x_i, β_{ii} is the quadratic effect of input factor x_i, and β_{ij} is the interaction coefficients effect between the input factors x_i and x_j.[4, 5] Consequently, a total of 30 experiments were randomly carried out using Design-Expert statistical software (Stat-Ease, Inc., USA) to evaluate the effects of parameters on decolorization efficiency.

Statistical analysis:

By applying the multiple regression analysis on the experimental data, a second-order polynomial equation is generated, which can express the relationship between process variables and the response. The final equation obtained in terms of coded factors is given below:

$$\begin{aligned}\text{Decolorization efficiency} =& 199.77 - 6.45X_1 + 0.05X_2 - 57.49X_3 \\ & - 0.17X_4 - 0.02X_1X_2 + 2.26X_1X_3 + 0.02X_1X_4 + 0.20X_2X_3 - 1.87\text{E} \\ & -003X_2X_4 + 0.47X_3X_4 + 0.03X_1^2 - 5.38\text{E-}004X_2^2 + 0.45X_3^2 - 5.61\text{E} \\ & -003X_4^2 - 4.90\text{E-}003X_1X_2\text{X}_3 + 5.72\text{E-}004X_1X_2X_4 - 0.020736X_1X_3X_4 \\ & -1.30167\text{E-}003X_2X_3X_4 \end{aligned} \quad (4)$$

In this polynomial expression, the negative coefficients of the quadratic terms signify their negative influences on the dye removal efficiency.[6]

CCD analysis:

The complete experimental design matrix and the responses based on experimental runs proposed by CCD with four factors in five levels for the photocatalytic decolorization of MB are given in Table S2. The model adequacy checking was performed on the experimental data to determine whether the approximating modal would give poor or misleading results. Four high degree polynomial models viz., linear, interactive (2FI), quadratic and cubic models were fitted to the experimental data. Furthermore, the coefficient of determination (R^2, Adj-R^2) was also utilized to evaluate the fitting quality of the polynomial model.[7] R^2 and Adj-R^2 were obtained by the following equations, respectively.

$$R^2 = 1 - \frac{SS_{\text{residual}}}{SS_{\text{model}} - SS_{\text{residual}}} \quad (5)$$

$$\text{Adj-}R^2 = 1 - \frac{SS_{\text{residual}} / DF_{\text{residual}}}{(SS_{\text{model}} + SS_{\text{residual}}) / (DF_{\text{model}} + DF_{\text{residual}})} \quad (6)$$

Where *SS* is the sum of squares, and *DF* is the degree of freedom. Three different test s namely, the sequential model sum of squares, lack of fit tests and model summary statistics, were carried out in this study to conclude the adequacy of models among various models to re present the maximum decolorization efficiency and the results are exhibited in Table S3. From Table S3, quadratic model was found to have maximum R^2, Adj-R^2, Pred-R^2 [7] and this is the most suitable model for the photocatalytic decolorization of MB. The "Pred-R^2" of 0.93 is in reasonable agreement with the "Adj-R^2" of 0.99 and indicating a good predictability of the model. Furthermore, the value of adjust ed R^2 was in accordance with the value of R^2 with regard to the sample size and the number of variables and statistical terms were based on the degrees of freedom.[8]

In addition, the obtained value of R^2 (0.9976) showed that 99.76% of the vari ations for the decolorization efficiency (%) could be accounted for by the model and the model could not explain only 0.24% of the variations.

Table S2. Experimental conditions and results of CCD

Run	MB concentration (mg L^{-1}) (X_1)	Catalyst dosage (mg/100 ml) (X_2)	pH (X_3)	Irradiation time (min) (X_4)	Actual value	Predicted value	Residual
1	17.5	100	6	75	73.56	72.77	0.79
2	11.25	125	4	97.5	90.10	90.08	0.020
3	17.5	150	6	75	86.03	83.83	2.20
4	11.25	175	8	52.5	93.27	93.32	-0.049
5	30	150	6	75	79.21	78.28	0.93
6	17.5	150	10	75	86.87	86.54	0.33
7	11.25	175	4	52.5	93.33	93.20	0.13
8	23.75	175	8	97.5	69.51	69.73	-0.22
9	23.75	125	8	52.5	82.62	83.20	-0.58
10	11.25	175	8	97.5	100.00	99.75	0.25
11	11.25	175	4	97.5	97.59	97.51	0.077
12	17.5	150	6	75	83.15	83.83	-0.68
13	17.5	150	6	120	77.41	77.33	0.076
14	11.25	125	8	97.5	87.85	88.01	-0.16
15	17.5	200	6	75	92.06	92.20	-0.14
16	23.75	175	4	97.5	98.20	98.25	-0.047
17	17.5	150	6	75	83.35	83.83	-0.48
18	23.75	125	8	97.5	62.83	63.11	-0.28
19	17.5	150	6	30	68.18	67.60	0.58
20	17.5	150	6	75	83.61	83.83	-0.22
21	17.5	150	6	75	83.51	83.83	-0.32
22	11.25	125	4	52.5	84.05	84.33	-0.28
23	23.75	125	4	52.5	70.54	70.95	-0.41
24	17.5	150	6	75	83.31	83.83	-0.52
25	23.75	175	8	52.5	86.71	86.88	-0.17
26	17.5	150	2	75	95.98	95.65	0.33
27	11.25	125	8	52.5	68.32	68.43	-0.11
28	23.75	175	4	52.5	70.51	70.86	-0.35
29	23.75	125	4	97.5	83.22	83.68	-0.46
30	5	150	6	75	100.00	100.00	0.00

Table S3. Sequential model fitting for the photocatalytic decolorization

Source	Sum of squares	df	Mean square	*F* value	*p*-value Prob>*F*	Remarks
Sequential model sum of squares						
Mean	2.108E+005	1	2.108E+005			
Linear	1558.46	4	389.61	6.54	0.0010	Suggested
2FI	372.61	6	62.10	1.06	0.4217	
Quadratic	426.87	4	106.72	2.32	0.1044	
Cubic	682.72	8	85.34	80.98	< 0.0001	Aliased
Residual	7.38	7	1.05			
Total	2.139E+005	30	7128.98			
Lack of fit tests						
Linear	1483.62	20	74.18	62.30	0.0001	Suggested
2FI	1111.01	14	79.36	66.64	0.0001	
Quadratic	684.14	10	68.41	57.45	0.0002	
Cubic	1.42	2	0.71	0.60	0.5852	Aliased
Pure Error	5.95	5	1.19			

Source	Std. Dev.	R^2	Adj-R^2	Pred-R^2	PREES	Remarks
Model summary statistics						
Linear	7.72	0.5113	0.4331	0.2374	2324.53	Suggested
2FI	7.67	0.6335	0.4407	-0.4608	4452.43	
Quadratic	6.78	0.7736	0.5623	-0.2957	3949.22	
Cubic	1.03	0.9976	0.9900	0.9300	213.51	Aliased

Analysis of variance (ANOVA):

The suggested model adequacy was checked further using ANOVA and the results are shown in Table S4. The significance of the model terms was evaluated based upon the *F* probability Prob > *F* at 95% confidence level.[9] The Model *F*-value of 199.63 suggests that the model is significant. There is only a 0.01% chance that a "Model *F*-value" of this value could be due to noise. It has to be noted that "Prob > *F*" values less than 0.05 indicate that the model terms are significant, whereas values more than 0.1 indicate the model terms are not significant. [10] In the present case, all factors, in terms of the linear, interaction and quadratic terms, were significant except for the interaction of pH and initial MB concentration term, which has a value more than 0.05 but less than 0.1. The F-value's of "Lack-of-Fit" is 0.47 that suggests that the Lack-of-Fit is not significant relative to the pure error.

Table S4. Analysis of variance regression model for MB photocatalytic decolorization

Source	Sum of Squares	df	Mean Square	F Value	p-value Prob > F
Model	3038.73	18	168.82	199.63	< 0.0001
X_1	725.45	1	725.45	857.84	< 0.0001
X_2	566.38	1	566.38	669.75	< 0.0001
X_3	124.47	1	124.47	147.19	< 0.0001
X_4	142.16	1	142.16	168.10	< 0.0001
X_1X_2	49.53	1	49.53	58.56	< 0.0001
X_1X_3	1.67	1	1.67	1.98	0.1875
X_1X_4	68.85	1	68.85	81.41	< 0.0001
X_2X_3	16.30	1	16.30	19.28	0.0011
X_2X_4	0.57	1	0.57	0.67	0.4306
X_3X_4	235.70	1	235.70	278.71	< 0.0001
X_1^2	50.91	1	50.91	60.20	< 0.0001
X_2^2	3.10	1	3.10	3.67	0.0817
X_3^2	90.63	1	90.63	107.16	< 0.0001
X_4^2	221.25	1	221.25	261.63	< 0.0001
$X_1X_2X_3$	37.55	1	37.55	44.40	< 0.0001
$X_1X_2X_4$	64.76	1	64.76	76.58	< 0.0001
$X_1X_3X_4$	544.17	1	544.17	643.48	< 0.0001
$X_2X_3X_4$	34.31	1	34.31	40.57	< 0.0001
Residual	9.30	11	0.85		
Lack of Fit	3.35	6	0.56	0.47	0.8084
Pure Error	5.95	5	1.19		
Cor Total	3048.04	29			

Diagnostics of model adequacy:

The investigation of the residual was conducted to validate the adequacy of the model. The plots of externally studentized residual versus the predicted responses are illustrated in Fig. S8a. The predicted values were randomly scattered within a constant range of residuals across the graph, which indicated that the proposed model and constant variance assumption were suitable. Also, externally studentized residuals versus run number plot (Fig. S8b) demonstrates that all the data points lay within the limits, which indicated the satisfactory fit of the developed model. The plots of predicted removal efficiency (%) versus experimental

decolorization efficiency for MB has been described in Fig. S8c. There was a good agreement between the predicted and experimental values. Fig. S8d illustrates a Box–Cox plot, which can be helpful for calculating the best power law transformation. From the Box–Cox plot for power transforms, lambda value of nearly one, suggests that no transformation is recommended for the response used (Fig. S8d). Cook's distance values (<0.50) demonstrate that our model does not have influence points.[11]

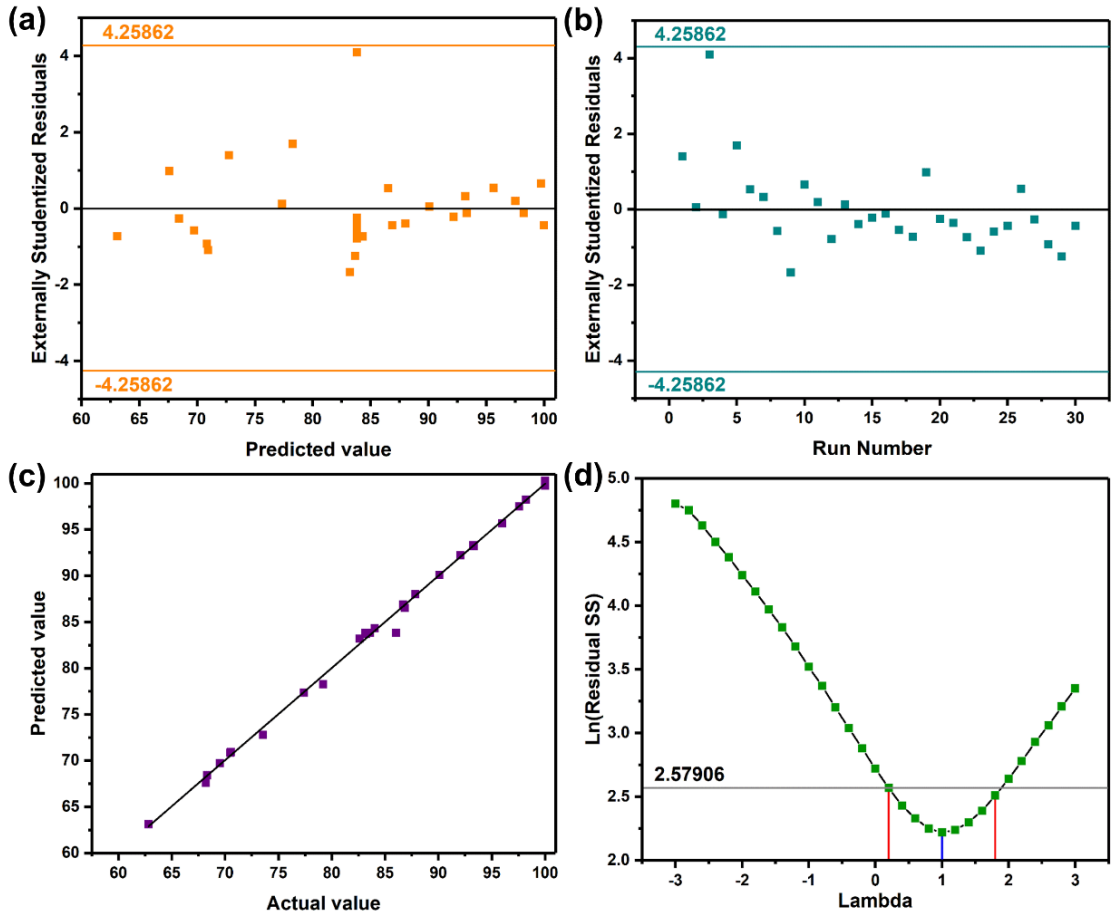

Fig. S8. Plot of (a) externally studentized residual vs predicted response, (b) externally studentized residual vs run number, (c) predicted removal efficiency versus experimental removal efficiency, and (d) Box–Cox plot for power transforms.

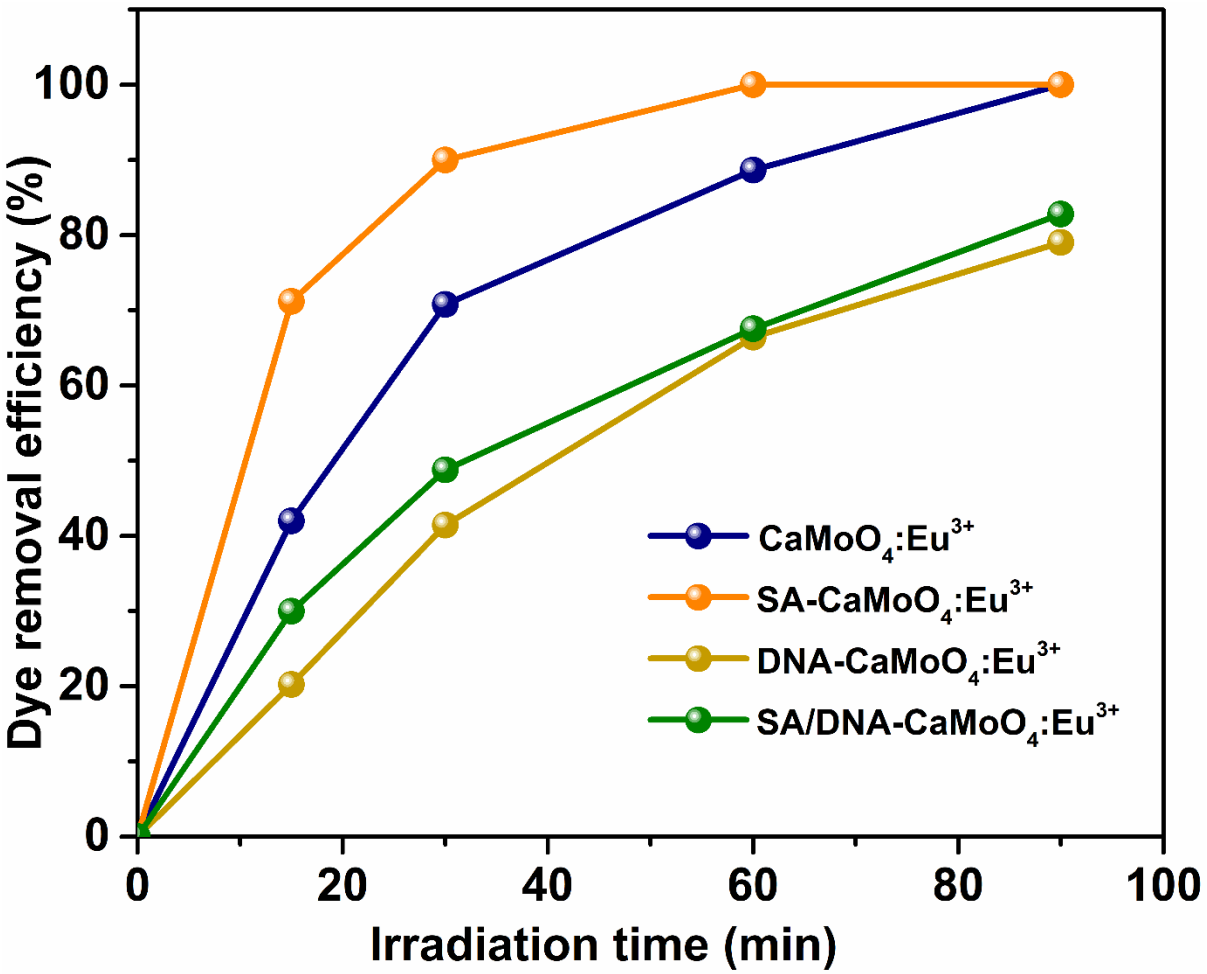

Fig. S9. Comparison between the dye removal efficiencies of $CaMoO_4:Eu^{3+}$ host, SA-$CaMoO_4:Eu^{3+}$, DNA-$CaMoO_4:Eu^{3+}$ and SA/DNA-$CaMoO_4:Eu^{3+}$ samples.

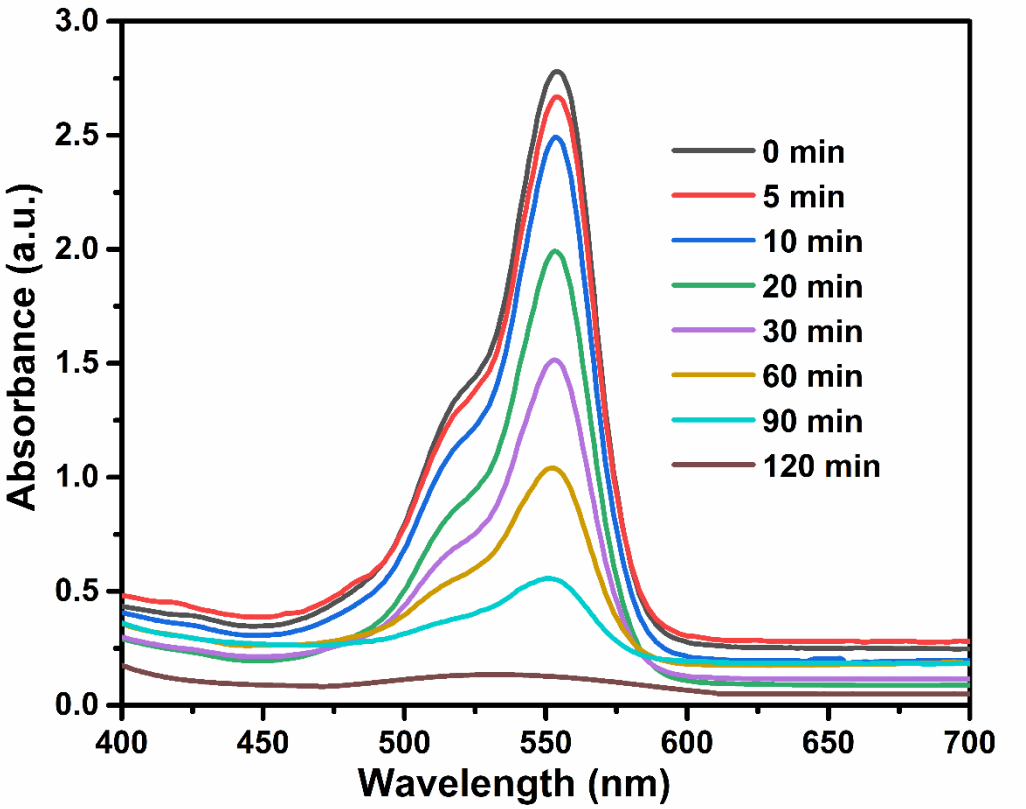

Fig. S10. The absorption spectra of RhB decolorized by SA-$CaMoO_4$:Eu^{3+} samples under UV irradiation at different time intervals.

Structural stability evaluation

To study the stability of the SA-$CaMoO_4$:Eu^{3+} against the photocorrosion, a series of photostability experiments have been conducted. The results of XPS and FTIR measurements before and after the decolorization of MB are shown in Fig. S11a & S11b, respectively. From the survey scan spectra and high-resolution spectra of all the elements presented in Fig. S11a & S11a(i-iv), we noticed that the peaks of Ca ($2p_{3/2}$ & $2p_{1/2}$), Mo($3d_{5/2}$ & $3d_{3/2}$), Eu ($3d_{5/2}$ & $3d_{3/2}$), and O(1s) are clearly visible after decolorization without any shifting. Surprisingly, no new peaks, however, were observed after the photocatalytic process, implying the high chemical stability of SA-$CaMoO_4$:Eu^{3+}.

Moreover, Fig. S11b displays the comparison of FTIR spectra of SA-$CaMoO_4$:Eu^{3+} before and after photocatalytic decolorization. When comparing FTIR spectra before and after photocatalytic process, all significant peaks remain unchanged, demonstrating no change observed in the functional groups present on SA-$CaMoO_4$:Eu^{3+}. In addition, it was found that there is no sign of MB in FTIR spectra after decolorization. This indicates that the decolorization of MB solution is derived from photocatalytic process rather than absorption.

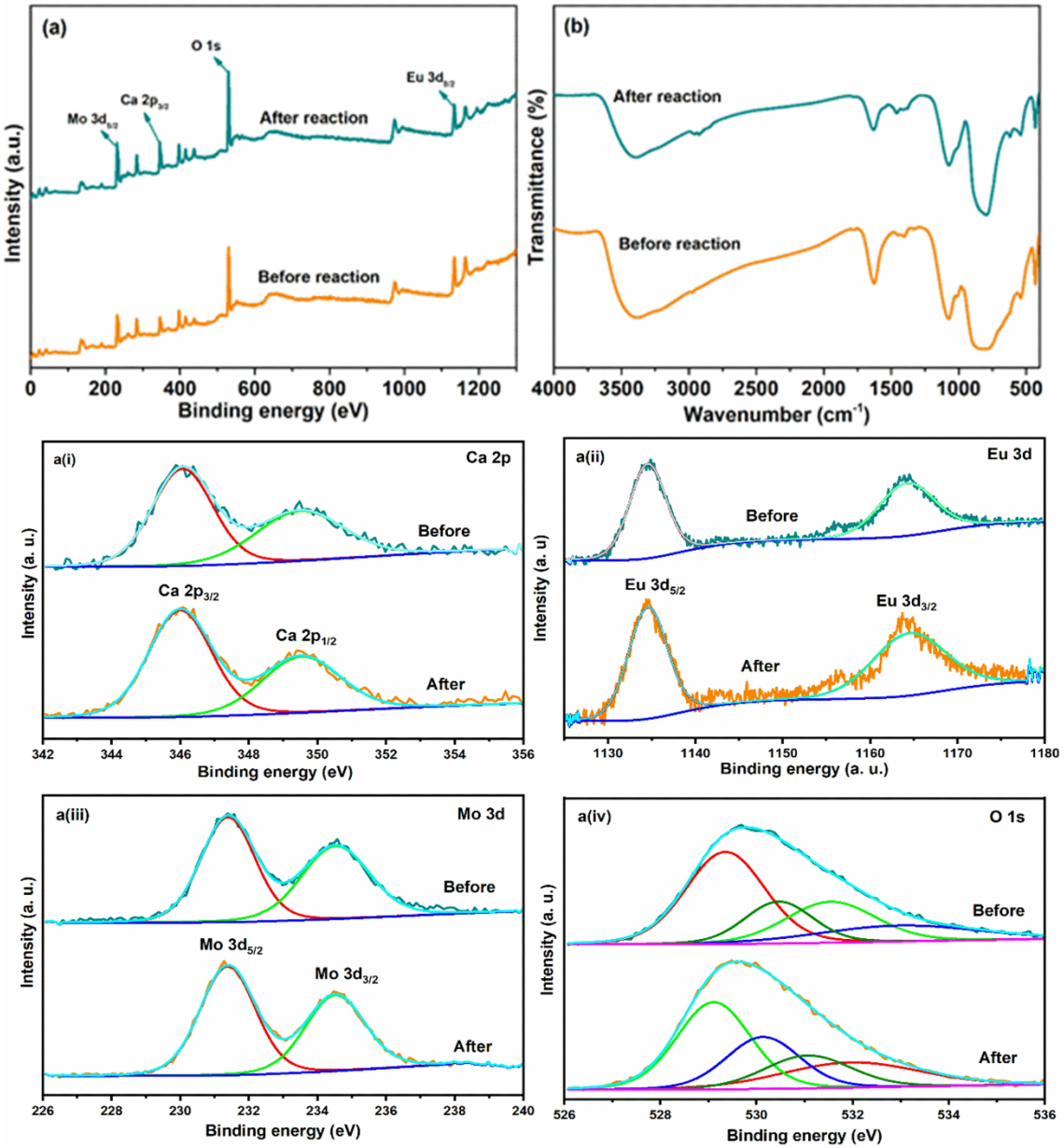

Fig. S11. (a) XPS and (b) FTIR spectra of SA-$CaMoO_4$:Eu^{3+} sample before and after decolorization (a(i), (ii), (iii) & (iv) displays the high-resolution XPS spectra of Ca 2p, Eu 3d, Mo 3d, and O1s elements respectively).

The morphology and luminescence properties of the SA-$CaMoO_4:Eu^{3+}$ microstructures before and after decolorization were presented in Fig. S12. As shown in Fig. S12b, some of the particles were broken after photocatalytic decolorization process as compared to the as-synthesized particles (Fig. S12a), but the membrane-bound-like morphology still remained the same. Likewise, when compared the PL emission spectra of SA-$CaMoO_4:Eu^{3+}$ microstructures before and after decolorization process, the profile and position of the band remains unchanged while the intensity of the band was slightly reduced for after reaction sample which is negligible.

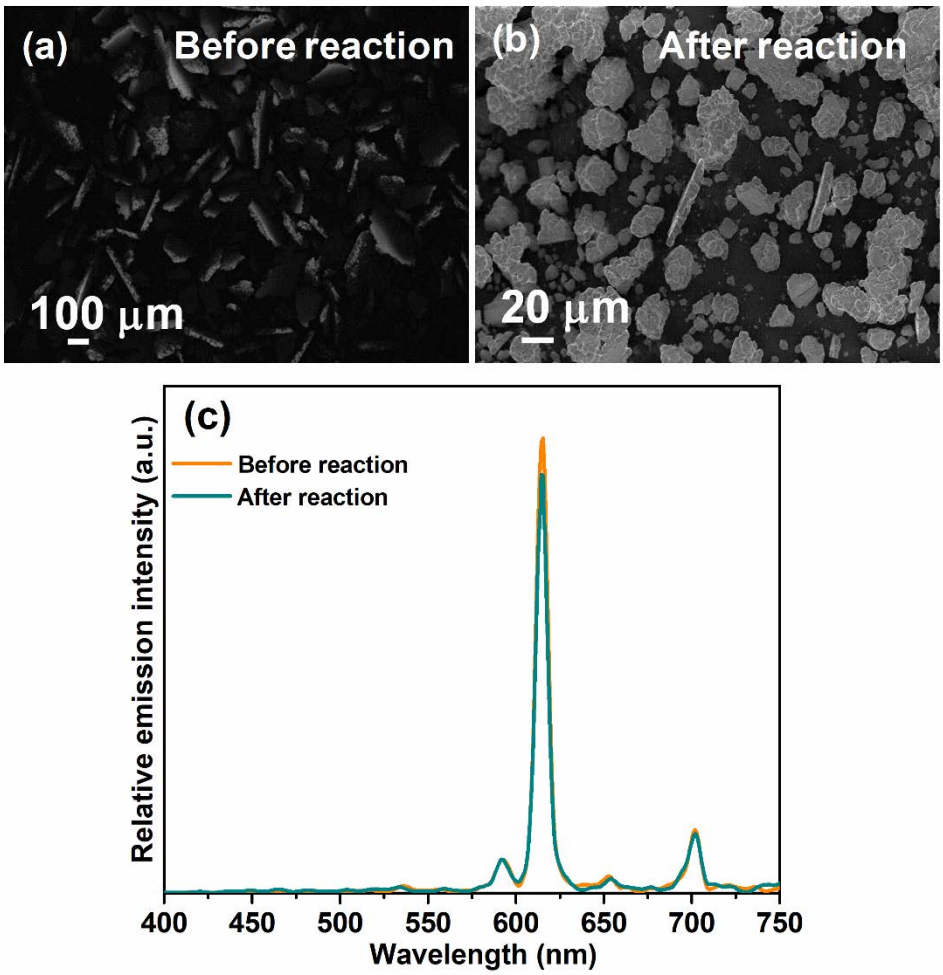

Fig. S12. FE-SEM images of the SA-$CaMoO_4:Eu^{3+}$ sample before (a) and after (b) decolorization process. (c) PL emission spectra of the SA-$CaMoO_4:Eu^{3+}$ before and after decolorization.

References:

1. A. Sassolas, B. D. Leca-Bouvier and L. J. Blum, *Chem. Rev.*, 2008, **108**, 109-139.

2. K.-R. Kim, D.-R. Kim, T. Lee, J. Y. Yhee, B.-S. Kim, I. C. Kwon and D.-R. Ahn, *Chem. Commun.*, 2013, **49**, 2010-2012.

3. I.-H. Cho and K.-D. Zoh, *Dyes Pigm.*, 2007, **75**, 533-543.

4. B. Kayan and B. Gözmen, *J. Hazard. Mater.*, 2012, **201**, 100-106.

5. P. Tripathi, V. C. Srivastava and A. Kumar, *Desalination*, 2009, **249**, 1273-1279.

6. S. M. Ghoreishian, K. Badii, M. Norouzi and K. Malek, *Appl. Surf. Sci.*, 2016, **365**, 252-262.

7. A. Özer, G. Gürbüz, A. Çalimli and B. K. Körbahti, *Chem. Eng. J.*, 2009, **146**, 377-387.

8. A. Hassani, A. Khataee, S. Karaca, M. Karaca and M. Kıranşan, *J. Environ. Chem. Eng.*, 2015, **3**, 2738-2749.

9. A. R. Soleymani, J. Saien, S. Chin, H. A. Le, E. Park and J. Jurng, *Process Saf. Environ. Prot.*, 2015, **94**, 307-314.

10. A. Aghaeinejad-Meybodi, A. Ebadi, S. Shafiei, A. Khataee and M. Rostampour, *J. Taiwan Inst. Chem. Eng.*, 2015, **48**, 40-48.

11. N. Tzikalos, V. Belessi and D. Lambropoulou, *Environ. Sci. Pollut. Res.*, 2013, **20**, 2305-2320.